High-harmonic and single attosecond pulse generation using plasmonic field enhancement in ordered arrays of gold nanoparticles with chirped laser pulses

Ying-Ying Yang[1,9] Armin Scrinzi,[2] Anton Husakou,[3] Qian-Guang Li,[4] Sarah L. Stebbings,[5] Frederik Süßmann,[5] Hai-Juan Yu,[1] Seungchul Kim,[6] Eckart Rühl,[7] Joachim Herrmann,[3] Xue-Chun Lin,[1] and Matthias F. Kling[5,8,10]

[1]*Laboratory of solid state laser sources, Institute of Semiconductors, Chinese Academy of Sciences, Beijing, 100083, China*

[2]*Ludwig-Maximilians Universität, Theresienstrasse 37, D-80333 Munich, Germany*

[3]*Max Born Institute of Nonlinear Optics and Short Pulse Spectroscopy, Max Born Strasse 2a, D-12489 Berlin, Germany*

[4]*Department of Physics, Hubei engineering University, University, Xiaogan, 432000, China*

[5]*Max-Planck-Institut für Quantenoptik, Hans-Kopfermann-Str. 1, D-85748 Garching, Germany*

[6]*Max Planck Center for Attosecond Science (MPC-AS), POSTECH, San 31, Hyoja-Dong, Namku, Pohang, Kyungbuk 790-784, South Korea*

[7]*Institut für Chemie und Biochemie - Physikalische und Theoretische Chemie, Freie Universität Berlin, Takustr. 3, D-14195 Berlin, Germany*

[8]*J.R. Macdonald Laboratory, Physics Department, Kansas-State University, 116 Cardwell Hall, Manhattan, Kansas 66506, USA*

[9]*yangyy@semi.ac.cn*

[10]*kling@phys.ksu.edu*

Abstract: Coherent XUV sources, which may operate at MHz repetition rate, could find applications in high-precision spectroscopy and for spatio-time-resolved measurements of collective electron dynamics on nanostructured surfaces. We theoretically investigate utilizing the enhanced plasmonic fields in an ordered array of gold nanoparticles for the generation of high-harmonic, extreme-ultraviolet (XUV) radiation. By optimization of the chirp of ultrashort laser pulses incident on the array, our simulations indicate a potential route towards the temporal shaping of the plasmonic near-field and, in turn, the generation of single attosecond pulses. The inherent effects of inhomogeneity of the local fields on the high-harmonic generation are analyzed and discussed. While taking the inhomogeneity into account does not affect the optimal chirp for the generation of a single attosecond pulse, the cut-off energy of the high-harmonic spectrum is enhanced by about a factor of two.

OCIS codes: (240.6680) Surface plasmons; (320.7110) Ultrafast nonlinear optics.

References and links

1. A. L'Huillier, L. A. Lompre, G. Mainfray, and C. Manus, "Multiply charged ions formed by multiphoton absorption processes in the continuum," Phys. Rev. Lett. **48**(26), 1814–1817 (1982).
2. P. B. Corkum, "Plasma perspective on strong field multiphoton ionization," Phys. Rev. Lett. **71**(13), 1994–1997 (1993).
3. F. Krausz and M. Ivanov, "Attosecond physics," Rev. Mod. Phys. **81**(1), 163–234 (2009).
4. G. Sansone, L. Poletto, and M. Nisoli, "High-energy attosecond light sources," Nat. Photonics **5**(11), 655–663 (2011).
5. M. Schultze, M. Fiess, N. Karpowicz, J. Gagnon, M. Korbman, M. Hofstetter, S. Neppl, A. L. Cavalieri, Y. Komninos, Th. Mercouris, C. A. Nicolaides, R. Pazourek, S. Nagele, J. Feist, J. Burgdörfer, A. M. Azzeer, R. Ernstorfer, R. Kienberger, U. Kleineberg, E. Goulielmakis, F. Krausz, and V. S. Yakovlev, "Delay in photoemission," Science **328**(5986), 1658–1662 (2010).

#179829 - $15.00 USD Received 13 Nov 2012; revised 23 Dec 2012; accepted 24 Dec 2012; published 22 Jan 2013

6. G. Sansone, F. Kelkensberg, J. F. Pérez-Torres, F. Morales, M. F. Kling, W. Siu, O. Ghafur, P. Johnsson, M. Swoboda, E. Benedetti, F. Ferrari, F. Lépine, J. L. Sanz-Vicario, S. Zherebtsov, I. Znakovskaya, A. L'huillier, M. Y. Ivanov, M. Nisoli, F. Martín, and M. J. J. Vrakking, "Electron localization following attosecond molecular photoionization," Nature **465**(7299), 763–766 (2010).
7. M. I. Stockman, M. F. Kling, U. Kleineberg, and F. Krausz, "Attosecond nanoplasmonic-field microscope," Nat. Photonics **1**(9), 539–544 (2007).
8. A. L. Cavalieri, N. Müller, Th. Uphues, V. S. Yakovlev, A. Baltuška, B. Horvath, B. Schmidt, L. Blümel, R. Holzwarth, S. Hendel, M. Drescher, U. Kleineberg, P. M. Echenique, R. Kienberger, F. Krausz, and U. Heinzmann, "Attosecond spectroscopy in condensed matter," Nature **449**(7165), 1029–1032 (2007).
9. A. Vernaleken, J. Weitenberg, T. Sartorius, P. Russbueldt, W. Schneider, S. L. Stebbings, M. F. Kling, P. Hommelhoff, H.-D. Hoffmann, R. Poprawe, F. Krausz, T. W. Hänsch, and T. Udem, "Single-pass high-harmonic generation at 20.8 MHz repetition rate," Opt. Lett. **36**(17), 3428–3430 (2011).
10. D. C. Yost, T. R. Schibli, and J. Ye, "Efficient output coupling of intracavity high-harmonic generation," Opt. Lett. **33**(10), 1099–1101 (2008).
11. I. Pupeza, T. Eidam, J. Kaster, B. Bernhardt, J. Rauschenberger, A. Ozawa, E. Fill, T. Udem, M. F. Kling, J. Limpert, Z. A. Alahmed, A. M. Azzeer, A. Tünnermann, T. W. Hänsch, and F. Krausz, "Power scaling of femtosecond enhancement cavities and high-power applications," Proc. SPIE **7914**, 79141I, 79141I-13 (2011).
12. S. Kim, J. Jin, Y.-J. Kim, I.-Y. Park, Y. Kim, and S.-W. Kim, "High-harmonic generation by resonant plasmon field enhancement," Nature **453**(7196), 757–760 (2008).
13. I.-Y. Park, S. Kim, J. Choi, D.-H. Lee, Y.-J. Kim, M. F. Kling, M. I. Stockman, and S.-W. Kim, "Plasmonic generation of ultrashort extreme-ultraviolet light pulses," Nat. Photonics **5**(11), 677–681 (2011).
14. A. Husakou, F. Kelkensberg, J. Herrmann, and M. J. J. Vrakking, "Polarization gating and circularly-polarized high harmonic generation using plasmonic enhancement in metal nanostructures," Opt. Express **19**(25), 25346–25354 (2011).
15. A. Husakou, S. J. Im, and J. Herrmann, "Theory of plasmon-enhanced high-order harmonic generation in the vicinity of metal nanostructures in noble gases," Phys. Rev. A **83**(4), 043839 (2011).
16. S. L. Stebbings, F. Süßmann, Y. Y. Yang, A. Scrinzi, M. Durach, A. Rusina, M. I. Stockman, and M. F. Kling, "Generation of isolated attosecond extreme ultraviolet pulses employing nanoplasmonic field enhancement: optimization of coupled ellipsoids," New J. Phys. **13**(7), 073010 (2011).
17. M. Sivis, M. Duwe, B. Abel, and C. Ropers, "Nanostructure-enhanced atomic line emission," Nature **485**(7397), E1–E3 (2012).
18. S. Kim, J. Jin, Y.-J. Kim, I.-Y. Park, Y. Kim, and S.-W. Kim, "Kim et al. reply," Nature **485**(7397), E1–E3 (2012).
19. A. Baltuška, T. Udem, M. Uiberacker, M. Hentschel, E. Goulielmakis, Ch. Gohle, R. Holzwarth, V. S. Yakovlev, A. Scrinzi, T. W. Hänsch, and F. Krausz, "Attosecond control of electronic processes by intense light fields," Nature **421**(6923), 611–615 (2003).
20. E. Goulielmakis, M. Schultze, M. Hofstetter, V. S. Yakovlev, J. Gagnon, M. Uiberacker, A. L. Aquila, E. M. Gullikson, D. T. Attwood, R. Kienberger, F. Krausz, and U. Kleineberg, "Single-cycle nonlinear optics," Science **320**(5883), 1614–1617 (2008).
21. E. D. Palik, *Handbook of Optical Constants of Solids* (Academic, 1991).
22. A. Plech, V. Kotaidis, M. Lorenc, and J. Boneberg, "Femtosecond laser near-field ablation from gold nanoparticles," Nat. Phys. **2**(1), 44–47 (2006).
23. J. A. Fan, C. Wu, K. Bao, J. Bao, R. Bardhan, N. J. Halas, V. N. Manoharan, P. Nordlander, G. Shvets, and F. Capasso, "Self-assembled plasmonic nanoparticle clusters," Science **328**(5982), 1135–1138 (2010).
24. J. F. Li, Y. F. Huang, Y. Ding, Z. L. Yang, S. B. Li, X. S. Zhou, F. R. Fan, W. Zhang, Z. Y. Zhou, Y. Wu, B. Ren, Z. L. Wang, and Z. Q. Tian, "Shell-isolated nanoparticle-enhanced Raman spectroscopy," Nature **464**(7287), 392–395 (2010).
25. A. Taflove and S. C. Hagness, *Computational Electrodynamics: the Finite-Difference Time-Domain Method* (Artech House Publishers, 2004).
26. H. Gai, J. Wang, and Q. Tian, "Modified Debye model parameters of metals applicable for broadband calculations," Appl. Opt. **46**(12), 2229–2233 (2007).
27. M. D. Feit, J. A. Fleck, Jr., and A. Steiger, "Solution of the Schrödinger equation by a spectral method," J. Comput. Phys. **47**(3), 412–433 (1982).
28. K. J. Schafer, B. Yang, L. F. DiMauro, and K. C. Kulander, "Above threshold ionization beyond the high harmonic cutoff," Phys. Rev. Lett. **70**(11), 1599–1602 (1993).
29. V. C. Reed and K. Burnett, "Ionization of atoms in intense laser pulses using the Kramers-Henneberger transformation," Phys. Rev. A **42**(5), 3152–3155 (1990).
30. I. Yavuz, E. A. Bleda, Z. Altun, and T. Topcu, "Generation of a broadband XUV continuum in high-order-harmonic generation by spatially inhomogeneous fields," Phys. Rev. A **85**(1), 013416 (2012).
31. B. Fetic, K. Kalajdzic, and D. B. Milosevic, "High-order harmonic generation by a spatially inhomogeneous field," Ann. Phys., doi:10.1002/andp.201200184.
32. M. F. Ciappina, J. Biegert, R. Quidant, and M. Lewenstein, "High-order-harmonic generation from inhomogeneous fields," Phys. Rev. A **85**(3), 033828 (2012).

#179829 - $15.00 USD Received 13 Nov 2012; revised 23 Dec 2012; accepted 24 Dec 2012; published 22 Jan 2013

1. Introduction

High-harmonic generation (HHG) is a well-established process for producing ultrashort, extreme-ultraviolet pulses by direct frequency up-conversion of femtosecond, near-infrared pulses in noble gases [1]. HHG is commonly described as a three-step process [2] where a strong laser field first tunnel ionizes an atom or molecule (step 1), then the emitted electron is accelerated in the laser field (step 2) and finally, an XUV photon is created upon the recollision and recombination of the electron with the ion (step 3). HHG has facilitated the generation of attosecond pulses as well as tabletop sources of coherent XUV and soft X-ray radiation [3,4]. These sources find applications in a wide range of fields, e.g., time-resolved studies of electronic dynamics in atoms, molecules, nanostructures and solids [1–8].

Recent emphasis on HHG has been in the development of high-repetition-rate systems in the multiple-100-kHz or even MHz range which provide high average XUV power. The challenge here is to reach peak intensities of approximately 10^{13} W/cm^2 when focusing the laser pulses into a gas target for high-harmonic generation. Therefore, the generation of high-order harmonics has typically relied on femtosecond laser amplifier systems with repetition rates in the few kHz range. In order to generate femtosecond and attosecond light pulses at a MHz repetition rate, the field provided by MHz rate laser oscillators needs to be magnified by at least two orders of magnitude. Different approaches have been followed to achieve this goal. Vernaleken *et al.* recently reported on single-pass HHG with amplified femtosecond laser pulses at a repetition rate of 20.8 MHz [9]. Using a passive, external cavity allows high pulse powers without active amplification at high repetition rates [10,11]. This approach requires excellent cavity stabilization and efficient XUV output coupling, which are challenging to implement [11]. An alternative approach is based on plasmonic field enhancement via metallic bow-tie nanostructures or waveguides [12–16] which has resulted in the generation of XUV light at repetition rates reaching 75 MHz [12]. However, the results for bow-tie nanostructures were recently challenged by Sivis *et al*. who only observed an enhancement of multi-photon and strong-field fluorescence [17]. Kim *et al*. claim that the local rare gas pressures present at the bow-tie nanostructures are responsible for the different observations [18]. Also, the number of XUV emitters N is essential for the creation of coherent versus incoherent XUV light. The coherent process scales with N^2 while the incoherent only scales with N. Further studies will be required to resolve this dispute and to clearly identify the regimes for coherent versus incoherent XUV emission from such nanostructures.

Time-resolved studies require the generation of short pulses of XUV light, the duration of which determines the achievable temporal resolution. Here, obtaining isolated attosecond pulses is preferable to trains of attosecond pulses which last femtoseconds. The generation of isolated attosecond pulses requires techniques in which the XUV emission is restricted to a single event for the femtosecond driving laser pulse [19]. This condition can be met with existing methods, e.g., by using a linearly polarized driving pulse with a duration of only a few optical cycles in combination with spectral filtering. Spectrally selecting the high-energy part near the cutoff of the resulting XUV light has resulted in the generation of pulses with 80 attosecond duration [20].

Here, we have studied high-harmonic radiation utilizing the enhanced near-fields in an ordered array of gold nanoparticles (NPs). As an advantage over bow-tie nanostructures and other nanostructure arrangements that have been considered so far, a dense coverage of a substrate with nanoparticles can be realized, and this enables a larger number of emitters to contribute to HHG. Increasing the number of emitters can significantly enhance the coherent high-harmonic generation process versus non-coherent contributions to the generation of XUV light. We have investigated how the plasmonic near-field can be tailored by adjusting the chirp of the incident pulses and single attosecond pulses (SAP) generated.

#179829 - $15.00 USD Received 13 Nov 2012; revised 23 Dec 2012; accepted 24 Dec 2012; published 22 Jan 2013

2. Optimization of the optical properties of the gold nanoparticle array

We have optimized the nanoparticle diameter and arrangement within the array to support both a large field enhancement and a large interaction volume for high-harmonic generation. We employed the finite element method (FEM) using HFSS software (version 12.0) to carry out the numerical calculations, and the wavelength-dependent refractive index is taken from Palik's handbook [21]. A mesh grid with step size 0.2 nm is applied around the gap between nanoparticles to achieve a sufficient precision in the calculations of the plasmonic fields. For zero chirp, the incident laser is assumed to have a Gaussian temporal profile of 5-fs duration. The laser wavelength is centered at the 800 nm wavelength typical of a Ti:sapphire, femtosecond oscillator operating at MHz repetition rate. We assume a focused intensity of 10^{11} W/cm^2. At this intensity, damage to the nanoparticle array by melting or ablation can be avoided [18,22].

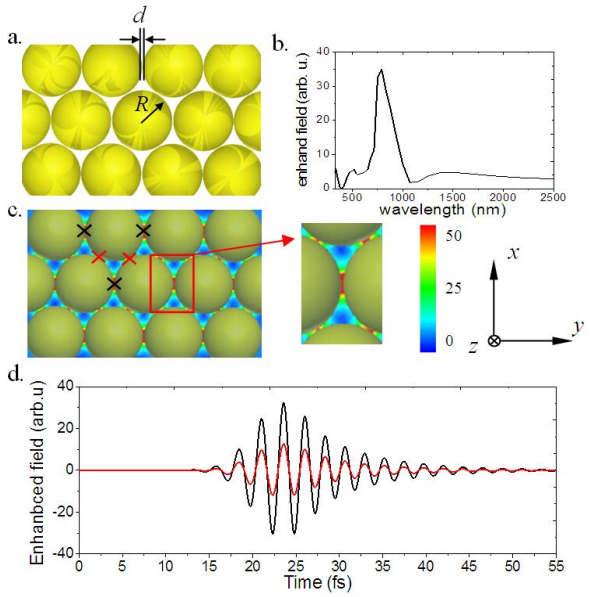

Fig. 1. (a) Schematic of the ordered gold NP array with an optimum radius of R = 80 nm and a gap between NPs of d = 2 nm; (b) Spectrum of the plasmonic field enhancement. The peak of the field enhancement was optimized to be at 800 nm; the observation point is at the center of the gap in the x-y plane and 15 nm above the cross-section of the NP array. The z-axis is 15 nm.(c) Contour plot of the enhanced fields between the nanoparticles; (d) The enhanced plasmonic field of three hot spots in the gaps (indicated by three black and two red crosses with corresponding color codes in (c)). The crosses are at 15 nm in z-axis.

The optimized, ordered array of gold NPs is shown in Fig. 1(a). In the simulation, the incident pulse propagates along the z-axis with polarization along the y-axis. These arrays are not as sensitive as bowtie nanostructures to the polarization of the incident laser pulse. Such an array can be fabricated by self-assembly employing colloidal chemistry methods [23,24] as can the gap between adjacent NPs which can be controlled very precisely (in the range of a few nanometers) by state-of-the-art methods [23]. This surpasses the spatial resolution of current lithographic techniques, and compared to the bowtie nanostructures employed in recent work [12,13], such arrays could be produced at low cost. We have chosen a gap size of d = 2 nm, which is both experimentally feasible and yields high field enhancement while providing a sufficiently large volume for HHG.

The plasmonic field enhancement spectrum of the NP array is shown in Fig. 1(b). The nanoparticle radius was optimized (to R = 80 nm) such that the peak of the field enhancement is at 800 nm, the central wavelength of the incident laser pulses. The observation point is at

#179829 - $15.00 USD Received 13 Nov 2012; revised 23 Dec 2012; accepted 24 Dec 2012; published 22 Jan 2013

the center of the gap in the x-y plane and 15 nm above the cross-section of the NP array. The maximum field enhancement exceeds 32 at this point and is higher towards the x-y plane. We chose a point 15 nm above the x-y plane as the observation point to facilitate sufficient field enhancement within at least 30 nm in z-direction. Within this region it can be assured that the intensities are enhanced by at least 10^3 times up to 10^{14} W/cm^2. Figure 1(c) shows the spatial distribution of the plasmonic field enhancement between the nanoparticles. The field enhancement factor exceeds 32 within a volume of 5.7×10^3 nm^3 obtained from numerical integration between adjacent NPs. Within this volume, the intensity of an incident pulse from a MHz oscillator is enhanced up to intensities exceeding 10^{14} W/cm^2, which is sufficient to generate high harmonics, e.g., in argon gas.

We may compare the efficiency of high-harmonic generation of the nanoparticle array with the bow-tie nanostructure geometry from Ref. [12]. For a field enhancement of 32, the enhanced volume of the bow tie geometry is $20 \times 50 \times 10$ nm^3 (this number was estimated from the calculations presented in Ref. [12]). If we assume that 100 bowties exhibit sufficient field enhancement for high-harmonic generation, they may contain 3.7×10^3 atoms at a local gas pressure of 115 torr. The enhanced volume is 5.7×10^3 nm^3 in the nanoparticle array geometry. Assuming a dense packing arrangement of 300 nanospheres within the same area as for the bowtie array (around 7.6 μm^2), the volume with sufficient field enhancement may contain 6.33×10^3 atoms and thus be more efficient than the bowtie nanostructure.

It should be noted that the focal intensity profile combined with the inhomogeneous field enhancement from the nanoparticle array creates an inhomogeneous intensity profile for high-harmonic generation. This aspect has not been considered in the current work. We have investigated the enhanced fields for various probe points within the array (see Fig. 1(d)) to test if the phase of the plasmonic fields is sensitive to the position of the gaps in the array. The fields from various probe points reveal a uniform phase of the enhanced plasmonic field which indicates that the emission of coherent XUV light is not limited by phase effects.

3. Tailoring the plasmonic field by chirped laser pulses

Recently, polarization gating has been proposed for the generation of an isolated attosecond XUV pulse via high-harmonic generation utilizing plasmonic field enhancement in cross-bow-tie nanostructures [14]. Here, we investigate another route towards the generation of isolated attosecond pulses which relies on the generation of a few-cycle, plasmonic near-field in combination with carrier-envelope phase control and appropriate spectral filtering of the resulting radiation. The approach is similar to the one discussed for coupled ellipsoids in [16]. In order to tailor the plasmonic near-field, however, we introduce in the current work a chirp parameter C in the incident laser field. The electric field of the incident pulse can be described as

$$E(t,C) = E_0 e^{-\frac{1+iC}{2}\left(2\sqrt{\ln 2}\frac{t}{\tau_p}\right)^2} e^{-i(\omega t+\varphi)} \qquad (1)$$

where τ_p is the pulse duration defined as full width at half maximum (FWHM) of a Gaussian envelope, E_0 is the field amplitude, ω is angular frequency, φ is the carrier-envelope phase (CEP), and C is the chirp parameter. This representation of the laser field was chosen in order to keep the laser spectrum constant when varying C. The simplest approach to introduce chirp into an experiment is by the insertion or removal of dispersive material into the laser path (which introduces a delay of the various spectral components without changing the spectrum). The chirp parameter C is varied from −1.5 to 1.5 with steps of 0.5. The resulting temporal structures of the laser pulses are displayed in Fig. 2(a). The pulse durations and field amplitudes for the chosen chirp parameters C are detailed in Table 1. As expected, an increase in the absolute value of C results in an increase in pulse duration and a decrease in field amplitude.

#179829 - $15.00 USD Received 13 Nov 2012; revised 23 Dec 2012; accepted 24 Dec 2012; published 22 Jan 2013

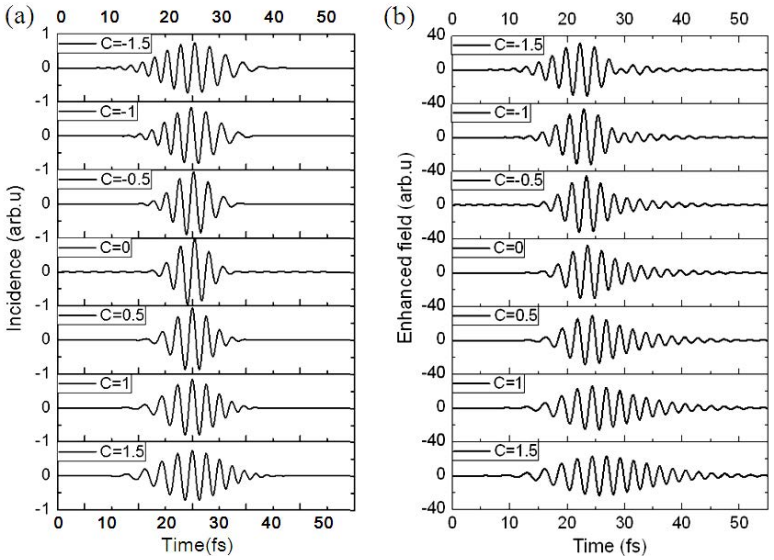

Fig. 2. (a) Temporal profiles of the incident laser pulse for different chirp parameters; (b) Corresponding enhanced plasmonic fields of the NP array. Note, that the CEPs of the fields for negative chirp in (a) and (b) have been optimized (see text for details).

Table 1. Incident laser pulse durations and peak field amplitudes for different chirp parameters. The peak field amplitude has been normalized to 1 for zero chirp.

Chirp parameter C	Pulse duration (fs)	Peak field amplitude (arb. units)	CEP
–1.5	9.0	0.74	$-\pi/3$
–1	7.1	0.84	$-5\pi/6$
–0.5	5.6	0.95	$5\pi/6$
0	5.0	1	$2\pi/3$
0.5	5.6	0.95	
1	7.1	0.84	
1.5	9.0	0.74	

The temporal profiles of the resulting enhanced plasmonic fields are simulated by the finite-difference time-domain (FDTD) method [25] employing the program FDTD solutions (Lumerical, version 7.0). The refractive index of gold that was used in the calculations is obtained from the modified Debye model [26]:

$$\varepsilon(\omega) = \varepsilon_i - \frac{\varepsilon_i - \varepsilon_s}{1 + i\tau\omega} + \frac{\sigma}{i\omega\varepsilon_0} \tag{2}$$

where ε_i is the infinite-frequency relative permittivity, ε_s is the static relative permittivity, τ is the relaxation time, σ is the conductivity, and ε_0 is the permittivity of free space.

Figure 2(b) shows the temporal profiles of the plasmonic near-fields for the chirp parameters corresponding to the pulses shown in Fig. 2(a). It is evident that when the parameter *C* increases, the maximum field enhancement and the decay time of the plasmonic fields change. Since the incident laser spectrum is not altered, the changes can be attributed to the effect of the chirp. The results can be distinguished by two parameter ranges:

1) When $C < 0$, i.e. negative chirp, the instantaneous frequency of the pulse decreases linearly and the nanostructure is off resonant after the time, where the maximum

#179829 - $15.00 USD Received 13 Nov 2012; revised 23 Dec 2012; accepted 24 Dec 2012; published 22 Jan 2013

field amplitude is reached, which efficiently reduces the remaining oscillations after the field maximum.

2) When $C > 0$, i.e. positive chirp, the instantaneous frequency of the pulse increases linearly and the nanostructure is in resonance at the time when the maximum amplitude is reached, resulting in a slow oscillatory decay of the near-field.

The creation of isolated, attosecond XUV pulses without gating techniques requires a few-cycle, near-field profile. Inspecting the profiles in Fig. 2(b), negative chirp provides a significantly better means to achieve this condition than positive chirp. We therefore focus our attention on negative chirp parameters in the following. We have optimized the CEP of the enhanced plasmonic fields in Figs. 2(a) and 2(b) for negative chirp to achieve the highest possible contrast between the peak field amplitudes of subsequent half-cycles. This is advantageous for single attosecond pulse generation as discussed below. The last column of Table 1 displays the optimum CEP values, which increase as the chirp parameter increases.

The generation of single-attosecond XUV pulses in conventional gas targets can be achieved by employing few-cycle light pulses with well-controlled CEP in combination with a band-pass filter selecting only the high-energy region of the XUV spectrum [19,20]. The photon energies of the XUV light created in HHG predominantly depend on the acceleration of the electron in the laser field. A high contrast between the field amplitudes of successive half-cycles of the laser field is desirable to isolate a single electron trajectory contributing to a chosen XUV photon energy range (resulting in a smooth, structure-less spectrum). Contributions from multiple trajectories result in interference becoming evident by a structured spectrum with characteristic peaks, e.g., at odd harmonics for rare gases. CEP-controlled, few-cycle pulses can exhibit a high field amplitude contrast between successive half-cycles of the laser field. Suitable adjustment of the CEP for a few-cycle pulse has therefore been sufficient to generate a smooth spectrum near the cutoff of the harmonic spectrum. Spectral filtering of this part of the spectrum, e.g., by a multilayer mirror, results in the isolation of an SAP. In our recent study on ellipsoid dimers, we have shown that the same approach can be applied to nanoplasmonic-field-enhanced HHG [16]. The study by Stebbings *et al*. has, however, shown that a single ellipsoid nanoparticle cannot provide sufficient field enhancement for HHG and the additional field enhancement present in coupled ellipsoid dimers is required [16]. Here, we investigate how SAPs can be generated in ordered arrays of spherical nanoparticles.

In order to meet the condition for the generation of a SAP, we have investigated the contrast between the main peak of the plasmonic field and the next largest adjacent peak. The CEP of the incident pulse has been adjusted in order to maximize this contrast in the plasmonic field for each chirp parameter. The resulting fields are displayed in Fig. 2(b). Table 2 shows the corresponding peak amplitudes and the contrast. We find the maximum field enhancement for $C = -0.5$ with a main peak to adjacent peak contrast of 1.30, which indicates that a pulse with this chirp might be most suitable for SAP generation. Although the peak contrast gives a first indication of the optimal conditions for SAP generation, further conclusions can only be drawn on the basis of calculations of the high-harmonic spectra and corresponding temporal profiles after spectral filtering.

Table 2. Parameters of plasmonic fields obtained with negatively chirped laser pulses

Chirp parameter C	CEP	Main peak amplitude (MPA)	Adjacent peak amplitude (APA)	Contrast (MPA/APA)
–1.5	-π/3	31.54	26.93	1.17
–1	–5π/6	33.31	26.42	1.26
–0.5	5π/6	33.89	26.15	1.30
0	2π/3	32.28	25.79	1.25

#179829 - $15.00 USD Received 13 Nov 2012; revised 23 Dec 2012; accepted 24 Dec 2012; published 22 Jan 2013

4. High-harmonic spectra and temporal profiles of resulting XUV pulses

The high-harmonic spectra are calculated from the plasmonic fields employing a split-operator method [27] to solve the one-dimensional, time-dependent Schrödinger equation. The time step is 2.77 attoseconds, which equals the time step in the FDTD calculations. In order to verify the convergence of the calculation, we compared the results to ones employing a smaller time step, and found no significant differences in the high-harmonic spectra. The calculations were performed within the single active electron approximation [28] and a soft-core potential [29] was adopted to compute the high-harmonic spectra from argon.

In Fig. 3(a), the calculated high-harmonic spectra are presented for an incident laser intensity of 10^{11}W/cm^2. The spectra exhibit a typical plateau and cutoff region with nearly constant and rapidly decreasing amplitude, respectively. The cutoff energy E_{cutoff} is classically given by

$$E_{cutoff} = 3.17U_p + I_p \tag{3}$$

where I_p is the ionization potential of the atom and U_p is the ponderomotive potential. When the chirp parameter C is varied from −1.5 to 0, the cutoff region shifts to higher energies (see Table 3). We obtained the energy range for the cutoff region from the spectra as follows: the plateau, the cutoff region and the region beyond the cutoff are linearly fitted (in the semi-logarithmic representation shown in Fig. 3(a)). The two crossing points of the three lines define the range of the cutoff region in Table 3.

Table 3. Parameters of the calculated HHG spectra

Chirp parameter C	Region of cutoff (eV)
−1.5	37-57
−1	38-58
−0.5	42-64
0	42-62

The number of cycles of the plasmonic field, which exhibit sufficient amplitude to drive the HHG process, directly affects the number of produced attosecond pulses. We have selected an appropriate spectral window to filter out the cutoff portion of the HHG spectrum and investigate if a SAP can be obtained.

Figure 3(b) shows the temporal profiles of the XUV pulses after spectral selection of the HHG cutoff regions from Fig. 3(a). For this process, Gaussian filters with FWHM of 5 eV and 10 eV are imposed. The filtered spectra were Fourier-transformed to obtain the temporal XUV pulse profiles shown in Fig. 3(b). The cleanest SAP is obtained for C = –0.5 for both filter functions. This confirms the simple contrast ratio analysis between the main peak and next largest adjacent peaks of the plasmonic field described above. The produced SAP has a Fourier-limited duration of 740 as and 490 as FWHM for the 5 eV and 10 eV filter respectively, obtained from a Gaussian fit of the temporal profiles. The results show that chirped pulses are very effective in tailoring the plasmonic fields and significantly help in the generation of SAPs using nanoplasmonic field enhancement.

#179829 - $15.00 USD Received 13 Nov 2012; revised 23 Dec 2012; accepted 24 Dec 2012; published 22 Jan 2013

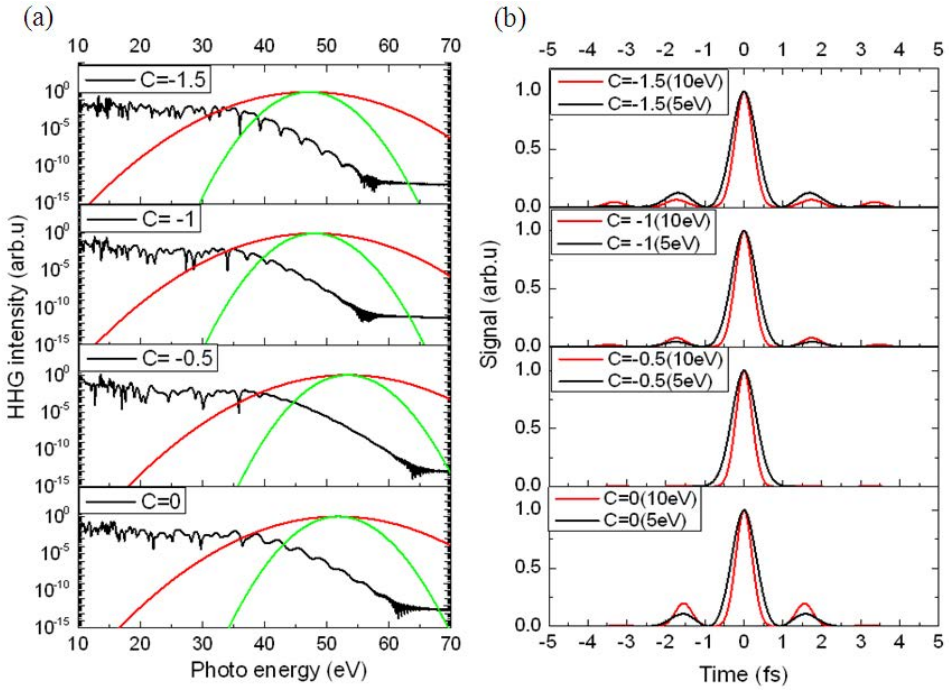

Fig. 3. (a) The HHG spectrum for an incident intensity of 10^{11} W/cm^2 (black line); the green line and the red line are the Gaussian band-pass filters with FWHM of 5 eV and10 eV, respectively. (b) Temporal profile of the generated XUV light after spectral selection of the cutoff region by a Gaussian filter of 5 eV FWHM (black line) and 10 eV FWHM (red line) in (a).

5. Effects of inhomogeneity of the enhanced fields

The motion of an electron in the gap between the nanoparticles is influenced by the presence of the metal interfaces. The electrons which collide with these interfaces are scattered or/and absorbed and are unlikely to contribute to the HHG process. Furthermore, the inhomogeneity of the electric field (due to the inhomogeneity of the field enhancement) influences the electron trajectories and thus the resulting high-harmonic spectrum. To study these effects, we utilize the model presented in Ref. [15]. This model is an extension of the semiclassical model using the strong-field approximation (Lewenstein model). The results obtained in this model, such as cutoff extension, are close to the results of more elaborate models by using the numerical solution of the time-dependent Schrödinger equation (see e.g., [30], [31].).

In Fig. 4 we present the dipole moment (a) and the harmonic spectrum of the dipole moment (b) calculated for a continuous wave incident beam with a higher incident intensity of 3×10^{11} W/cm^2 and wavelength of 882 nm. These parameters have been chosen to yield similar results when compared to the calculations above, as well as to identify HHG regimes characterized by the significant influence of the above-described effects. The observation point is 1 nm away from the metal surface at the center of the gap. The time-dependent dipole moment in (a) is highly asymmetric with respect to the y axis, and is reflected in the associated electron motion, which can subsequently travel only in the positive x direction. This manifests as - both odd and even harmonics, which in many regions of the spectrum have roughly the same amplitude. This is clearly a result of strongly-broken point symmetry in very close vicinity to a metal interface.

In spite of this, the gap between the spheres as a whole is symmetric as shown in Fig. 5(a), and one would not expect for the dipole moment symmetry (integrated over the interaction volume) to be broken. Also, the high-harmonic spectrum presented in Fig. 5(b) by the red

#179829 - $15.00 USD Received 13 Nov 2012; revised 23 Dec 2012; accepted 24 Dec 2012; published 22 Jan 2013

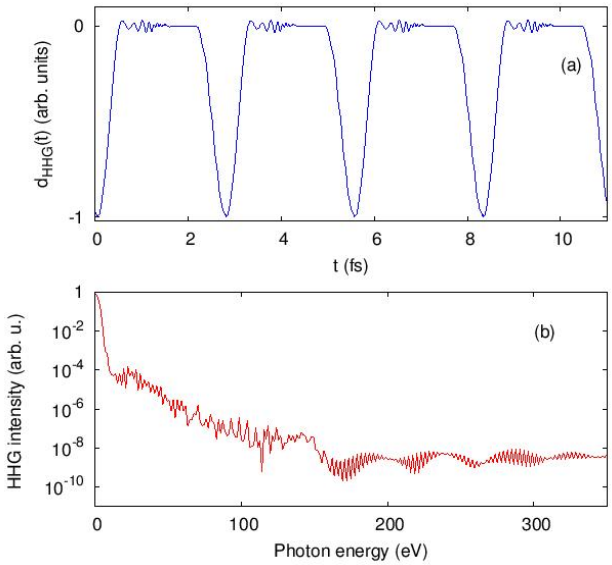

Fig. 4. The dipole moment (a) and the harmonic spectrum of the dipole moment (b) for a continuous wave incident beam at 882 nm with an intensity of 3×10^{11} W/cm^2. The observation point is 1 nm away from the metal surface at the center of the gap.

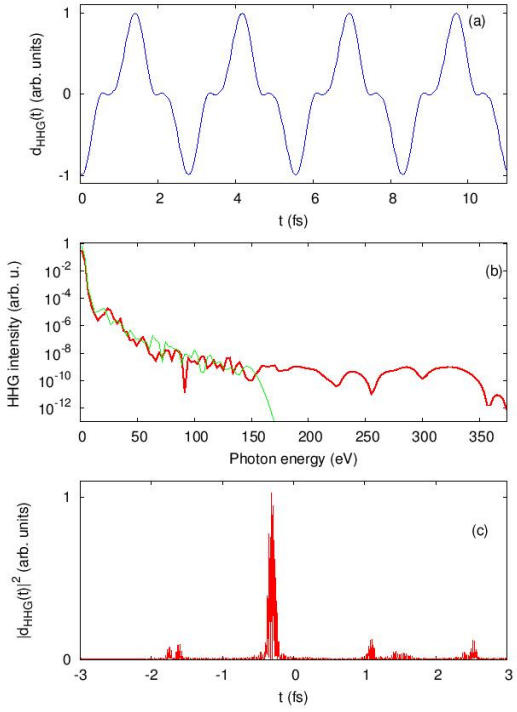

Fig. 5. (a) The total dipole momentum in the gap. (b) The high-harmonic spectrum, where the red curve is calculated by the model presented in Ref. [15], and the thin green curve is calculated by the standard model. (c) The temporal profile corresponding to selection of the cut-off region for a chirp parameter of C = –0.5.

#179829 - $15.00 USD Received 13 Nov 2012; revised 23 Dec 2012; accepted 24 Dec 2012; published 22 Jan 2013

surfaces and (to a lesser extent) the (near-)field inhomogeneities lead to a significant extension of the cutoff. In comparison with the standard model shown by the thin green curve in Fig. 5(b), the cutoff is more than doubled from ca. 148 eV to 339 eV. A similar extension in the cutoff position is also reported in Ref. [32]. The phases of the harmonics beyond the homogeneous-pump cutoff are close to the phases of the harmonics at the cutoff.

We have also studied the influence of the electron collisions with the metal surfaces and the enhancement inhomogeneity for an incident femtosecond pulse as defined by Eq. (1) for the chirp parameter $C = -0.5$. The results shown in Fig. 5(c) indicate that the generation of a SAP is not influenced by the two effects shown above, even at a higher intensity of 3×10^{11} W/cm^2. A single attosecond pulse with some side lobes and a FWHM duration of 120 attoseconds is predicted in this case for the range from 128 eV to 170 eV. This range was optimized to produce short and intense SAP with top-hat function as a filter function.

6. Conclusions

We have investigated high-harmonic generation via nanoplasmonic field enhancement by an ordered array of gold nanospheres. Gold nanospheres can be fabricated by colloidal chemistry methods in large quantities and with high accuracy. For an ordered array with spherical nanoparticles with radius $R = 80$ nm and a minimum distance between the nanoparticles of $d = 2$ nm in a hexagonal dense packing arrangement we find an enhancement factor of about 32 within a 5.7×10^3 nm^3 volume between nanoparticles. This volume could contain 6.33×10^3 atoms at a local gas pressure of 115 torr and exceed the conditions for the bow-tie nanoarray used in Ref. [12]. We have investigated the impact of the chirp of incident femtosecond laser pulses on the high-harmonic generation in argon. Our results indicate that a single attosecond pulse can be obtained by tailoring the chirp of the laser field, adjusting the CEP, and spectrally selecting the high energy part of the spectrum near the cutoff. We have also investigated the influence of inhomogeneity of the enhanced fields. We find that the inhomogeneity does not affect the optimal chirp conditions for the generation of a SAP, but leads to an enhancement of the cut-off by roughly a factor of two.

Acknowledgments

Financial support from the Chemical Sciences, Geosciences, and Biosciences Division, Office of Basic Energy Sciences, Office of Science, U.S. Department of Energy under DE-SC0008146 and DE-FG02-86ER13491; the BMBF via PhoNa; the DFG via Kl-1439/4 and Kl-1439/5; the Cluster of Excellence: Munich Center for Advanced Photonics (MAP); the National Science Foundation under EPS-0903806; and DFG project HU 1593/2-1 is acknowledged with thanks. We are furthermore grateful for support by the King-Saud University in the framework of the MPQ-KSU collaboration and the visiting professor program.

#179829 - $15.00 USD Received 13 Nov 2012; revised 23 Dec 2012; accepted 24 Dec 2012; published 22 Jan 2013